Hybrid Semiconducting Polymer Dot–Quantum Dot with Narrow-Band Emission, Near-Infrared Fluorescence, and High Brightness

ARTICLE *in* JOURNAL OF THE AMERICAN CHEMICAL SOCIETY · APRIL 2012

Impact Factor: 12.11 · DOI: 10.1021/ja3022973 · Source: PubMed

7 AUTHORS, INCLUDING:

Yang-Hsiang Chan
National Sun Yat-sen University
30 PUBLICATIONS **831** CITATIONS
SEE PROFILE

Fangmao Ye
University of Washington Seattle
30 PUBLICATIONS **716** CITATIONS
SEE PROFILE

Xuanjun Zhang
University of Macau
51 PUBLICATIONS **1,321** CITATIONS
SEE PROFILE

Yuhui Jin
University of Washington Seattle
26 PUBLICATIONS **1,134** CITATIONS
SEE PROFILE

Published in final edited form as:
J Am Chem Soc. 2012 May 2; 134(17): 7309–7312. doi:10.1021/ja3022973.

Hybrid Semiconducting Polymer Dot-Quantum Dot with Narrow-Band Emission, Near-Infrared Fluorescence, and High Brightness

Yang-Hsiang Chan, **Fangmao Ye**, **Maria Elena Gallina**, **Xuanjun Zhang**, **Yuhui Jin**, **I-Che Wu**, and **Daniel T. Chiu***
Department of Chemistry, University of Washington, Seattle, WA, 98195.

Abstract

This communication describes a new class of semiconducting polymer nanoparticle-quantum dot hybrid with high brightness, narrow emission, near-infrared fluorescence, and excellent cellular targeting capability. Using this approach, we circumvented the current difficulty with obtaining narrow-band emission and near-infrared fluorescing semiconducting polymer nanoparticles, while combining the advantages of both semiconducting polymer nanoparticles and quantum dots. We further demonstrated the use of this new class of hybrid nanomaterial for effective and specific cellular and subcellular labeling without any noticeable nonspecific binding. This hybrid nanomaterial is anticipated to find use in a variety of *in vitro* and *in vivo* biological applications.

There has been considerable effort in the design of nanostructured materials with highly integrated functionalities, because of their potential use in diverse applications, such as multimodality imaging, optoelectronics, and nanomedicine.[1–7] In particular, fluorescent inorganic nanoparticles (NPs), often referred to as quantum dots (Qdots), have attracted much attention in the past decade because of their unique optical features, including high quantum yields, large effective Stokes shifts, broad absorption with narrow emission in which the emission wavelength can be tuned by the size of Qdots.[8–12]

Recently, semiconducting polymer nanoparticles (Pdots) have emerged as a new class of highly fluorescent nanomaterials owing to their extraordinary fluorescence brightness, excellent photostability, and high emission rates.[13–28] There is, however, a significant drawback to Pdots at present, namely, most reported semiconducting polymers used for forming Pdots have broad emission bands.[13,17] This drawback greatly limits the multiplex capability of Pdots, because broad-band emission can result in spectral interference with other fluorophores, especially for Pdots with high brightness where leakage of emitted photons into other detection channels can easily overwhelm the fluorescence from other non-Pdot probes. Moreover, the synthesis of suitable near-IR fluorescing semiconducting polymers (700–1000 nm) for generating Pdots remains a difficult challenge, in part due to the self-quenching of NIR polymers upon condensation into a Pdot form.

A key aim in the design of hybrid nanomaterials is to enhance the beneficial signature properties of one component, while preserving the desired characteristics of the other(s). To demonstrate this concept and to address the above-mentioned drawbacks of Pdots, this

chiu@chem.washington.edu.

Supporting Information Available: Synthesis of PFBT with amino functional groups, Pdot-Qdot preparation and characterization, experimental section, cell culturing, and labeling, Figure S1–S5. This material is available free of charge via the Internet at http://pubs.acs.org.

communication reports a facile, versatile, and scalable strategy that can integrate the optical properties of both Qdots and Pdots without sacrificing their functionalities. The high brightness of Pdots is derived in part by the large absorption cross section of the semiconducting polymer. The Pdot-Qdot hybrid integrates the high absorption cross section offered by Pdots and the narrow emission and near-IR fluorescence available from Qdots. The approach is based on the replacement of the surfactants of CdSe Qdots by poly[9,9-dioctylfluorenyl-2,7-diyl)-co-1,4-benzo-{2,1'-3}-thiadiazole)] (PFBT) polymer derivative, followed by the co-nanoprecipitation of the functionalization polymers, semiconducting polymers, and CdSe Qdots to form the final Pdot-Qdot hydrid.

Figure 1A outlines our strategy in more detail, where we synthesized PFBT with amino functional groups so that we could convert these amino groups to thiols using 2-iminothiolane (Traut's reagent) in THF in an effort to have an efficient ligand-exchange process with the original amino capping ligands on the Qdot surface. After the ligand exchange reaction, we blended PFBT with a copolymer, PS-PEG-COOH that comprised the carboxyl groups needed for further bioconjugation of Pdots. The polymer-Qdot solution was co-precipitated in water under sonication to form the final Pdot-Qdot NPs. It is worth mentioning that if 2-iminothiolane was not added during the ligand exchange process, the resulting Pdot-Qdot NPs aggregated with 12 hours, which demonstrated the importance of the conversion of amines to thiols in order to have an efficient ligand exchange between polymers and original amino capping ligands on Qdot surface. From transmission electron microscopy (TEM) images (Figure 1B), we can clearly see that a cluster of Qdots was encapsulated in the Pdot, in which there are ~30 Qdots embedded inside each individual hybrid nanoparticle. Dynamic light scattering (DLS) measurements also showed that the average diameter of Pdot-Qdot NPs was ~25 nm (Figure 1C).

It is worth mentioning that the crystalline structure of Qdots remained intact during the preparation processes (Figure 1B), which is important in preserving the optical properties of Qdots. Furthermore, this hybrid Pdot-Qdot remained optically stable and biologically active for at least two months of storage at 4°C in physiological pH buffers (*vide infra*). We noticed that the color of emission changed drastically from bright yellow fluorescence before nanoprecipitation to deep-red emission after nanoprecipitation. Because the yellow fluorescence is characteristic of PFBT, while the red fluorescence is from Qdots, this phenomenon is indicative of highly efficient energy transfer from PFBT to Qdots, which were in close contact after nanoprecipitation and formation of the Pdot-Qdot hybrid.

Figure 2A shows a typical absorption spectrum of Pdot-Qdot NPs. The absorption peak at ~450 nm (blue arrow) is from PFBT and the small absorption at ~640 nm (red arrow) is from CdSe Qdots, while the high absorption below 400 nm is attributed to both PFBT and Qdots. In the present work, we employed three different sizes of Qdots that emit at 655 nm (QD655), 705 nm (QD705), and 800 nm (QD800), respectively. These were commercially available (from Invitrogen). We carefully optimized the ratio of PFBT to Qdots (see Supporting Information) in order to have efficient energy transfer from PFBT to Qdots while aiming to have a compact size (i.e. minimal number of Qdots inside a Pdot). Therefore, different number of Qdots was encapsulated inside the Pdot for different sizes of Qdots that we employed. As shown in Figure 2B, the fluorescence emission of PFBT (black arrow) was almost completely quenched, indicating an efficient energy/electron transfer from PFBT to Qdots. We also measured the time-resolved fluorescence decay curves of QD655 and Pdot-QD655 (Figure S5) to further confirm the energy transfer between PFBT and Qdots.

More importantly, the emission bandwidth of Pdot-Qdot NPs remained unaltered when compared with the original Qdot emission, thereby allowing us to create Pdot-based NPs that retained the narrow emission characteristics of Qdots. Taking QD655 as an example, the

full width at half maximum of Pdot-QD655 in water is ~25 nm (solid red line in Figure 2B), which is essentially the same as the width of the original QD655 emission in decane (dashed red line). We also demonstrated that this technique can be applied to NIR Qdots, such as QD705 and QD800 (purple and pink lines in Figure 2B).

The quantum yields of Pdot-QD655, Pdot-QD705, and Pdot-QD800 in buffer solutions were determined to be 23%, 38%, and 29%, respectively, while the quantum yields of QD655, QD705, and QD800 after transferring from decane to aqueous solution were 27%, 41%, and 32%, respectively. This implies that we should be able to take advantage of the unique optical properties of Qdots such as narrow-band and NIR emission without sacrificing their high quantum yields, while implanting the merits of Pdots on them, including the large absorption cross-sections and facile surface functionalization offered by Pdots.

To understand the performance of the Pdot-Qdot NPs, we measured their single-particle fluorescence brightness (Figure 2C&2D). In our previous work, we have established that each single PFBT-DBT Pdot emitting at ~650nm is about 15 times brighter than each single QD655.[25] Therefore, here we directly compared the single-particle brightness of PFBT-DBT Pdots with PFBT-QD655 NPs. We found the particle brightness of PFBT-QD655 is comparable to that of PFBT-DBT (Figure 2C&2D), which suggests the particle brightness of PFBT-QD655 is in turn about 15 times brighter than that of single QD655. Because the particle brightness is given by the product of absorption cross section and quantum yield and because the quantum yields of QD655 and Pdot-QD655 were comparable, we can ascribe most of the brightness enhancement to the vast increase in the optical absorption cross section provided by the semiconducting polymer coating or/and Qdot multiples.

We next employed Pdot-Qdot for both cell-surface and subcellular labeling to demonstrate their potential in biological applications. In one experiment, we performed subcellular microtubule labeling in HeLa cells. Here, we first conjugated streptavidin onto the surface of Pdot-Qdot NPs *via* 1-ethyl-3-[3-dimethylaminopropyl]carbodiimide hydrochloride-(EDC)-catalyzed coupling (see Supporting Information). We then incubated Pdot-Qdot-streptavidin together with biotinylated monoclonal anti-α-tubulin antibody with HeLa cells so that Pdot-Qdot-streptavidin NPs could label the microtubules of HeLa cells. Figure 3A–3C shows representative confocal images of Pdot-QD705-streptavidin labeled microtubules in HeLa cells, indicating Pdot-Qdot-streptavidin could be specifically targeted onto subcellular structures in the presence of biotinylated antibody. However, due to the relative large particle size of Pdot-Qdot NPs, the tail regions of microtubules could not be well resolved (Figure 3A). To obtain particles with smaller sizes, if needed, further experimentation of suitable polymer-Qdot pairs is required. No noticeable fluorescence signal from Pdot-Qdot was observed for negative control samples (Figure 3D–3F) where the experimental conditions were identical as that in Figure 3A–3C except for the absence of the biotinylated primary antibody. These results indicate this new class of fluorescent hybrid probes exhibit highly specific binding activity with minimal nonspecific absorption.

Additionally, we also carried out flow cytometry experiments using Pdot-QD705 and Pdot-QD800 to label membrane proteins on MCF-7 cells. Here, the Pdot-Qdot-streptavidin conjugates, together with primary biotin anti-human CD326 EpCAM antibody and biotinylated goat anti-mouse IgG secondary antibody were labeled onto the surfaces of live MCF-7 cells. Pdot-QD705 and Pdot-QD800 have emissions in the NIR, which is beneficial in many biological studies. Figure 3G & 3H shows the flow cytometry results for Pdot-QD705 and Pdot-QD800, respectively. Both probes showed excellent separation between Pdot-Qdot-streptavidin labeled cells (purple/pink line, with primary antibody) and the negative control/background (black lines, without primary antibody). These results demonstrate Pdot-Qdot bioconjugates could be targeted to MCF-7 cells effectively and

specifically with ultralow nonspecific binding, consistent with the results from confocal microscopy in HeLa cells.

For practical applications and translation of the Pdot-Qdot hybrid for wide-spread adoption, the colloidal stability and storability of the Pdot-Qdot solution is important. To assess this aspect,, we stored the Qdot-embedded Pdots at 4 °C for two months in a buffer solution. We then used flow cytometry to evaluate the fluorescence of the labeled cells as well as the negative control, which would be affected by the presence of any non-specific absorption. As shown in Figure S2 (see Supporting Information), take Pdot-QD800-streptavidin for example, we observed a negligible change in the fluorescence of labeled MCF-7 cells and no increase in nonspecific binding, which indicates excellent colloidal stability and storability. Furthermore, no particle aggregation or size increase was found from DLS measurements after two months of storage (data not shown).

In summary, we have developed a new class of nanocomposites made of Pdots and Qdots, which exhibit combined functionalities and optical properties that are superior to either type of nanoparticle. The hybrid nanoparticles possess high brightness with narrow/NIR emission, easy optical tunability, and facile surface chemistry, which are not available simply from Pdots or Qdots alone. We envision this new nanocomposite can be utilized for a variety of biological applications, including specific *in vitro* and *in vivo* cellular imaging. In addition to bioimaging, by integrating with our recent advances in sensing physiologically important species using Pdots,[21,22,26] this hybrid nanomaterials should also afford a new means of biological or environmental analysis.

Supplementary Material

Refer to Web version on PubMed Central for supplementary material.

Acknowledgments

This work was supported by the National Institutes of Health (NS 062725 and CA147831) and the National Science Foundation (CHE-0844688).

REFERENCES

1. Jin Y, Gao X. Nat. Nanotechnol. 2009; 4:571–576. [PubMed: 19734929]
2. Hu S-H, Gao X. J. Am. Chem. Soc. 2010; 132:7234–7237. [PubMed: 20459132]
3. Zhang J, Tang Y, Lee K, Ouyang M. Science. 2010; 327:1634–1638. [PubMed: 20339071]
4. Jones MR, Osberg KD, Macfarlane RJ, Langille MR, Mirkin CA. Chem. Rev. 2011; 111:3736–3827. [PubMed: 21648955]
5. Donegá, CdM. Chem. Soc. Rev. 2011; 40:1512–1546. [PubMed: 20972490]
6. Behrens S. Nanoscale. 2011; 3:877–892. [PubMed: 21165500]
7. Buck MR, Bondi JF, Schaak RE. Nat. Chem. 2012; 4:37–44. [PubMed: 22169870]
8. Medintz IL, Uyeda HT, Goldman ER, Mattoussi H. Nat. Mater. 2005; 4:435–446. [PubMed: 15928695]
9. Somers RC, Bawendi MG, Nocera DG. Chem. Soc. Rev. 2007; 36:579–591. [PubMed: 17387407]
10. Choi HS, Liu W, Misra P, Tanaka E, Zimmer JP, Ipe BI, Bawendi MG, Frangioni JV. Nat. Biotechnol. 2007; 25:1165–1170. [PubMed: 17891134]
11. Michalet X, Pinaud FF, Bentolila LA, Tsay JM, Doose S, Li JJ, Sundaresan G, Wu AM, Gambhir SS, Weiss S. Science. 2005; 307:538–544. [PubMed: 15681376]
12. Derfus AM, Chan WCW, Bhatia SN. Nano Lett. 2004; 4:11–18.
13. Wu C, Bull B, Szymanski C, Christensen K, McNeill J. ACS Nano. 2008; 2:2415–2423. [PubMed: 19206410]

14. Howes P, Green M, Levitt J, Suhling K, Hughes M. J. Am. Chem. Soc. 2010; 132:3989–3996. [PubMed: 20175539]
15. Kaeser A, Schenning APH. J. Adv. Mater. 2010; 22:2985–2997.
16. Pecher J, Mecking S. Chem. Rev. 2010; 110:6260–6279. [PubMed: 20684570]
17. Tian Z, Yu J, Wu C, Szymanski C, McNeill J. Nanoscale. 2010; 2:1999–2011. [PubMed: 20697652]
18. Tuncel D, Demir HV. Nanoscale. 2010; 2:484–494. [PubMed: 20644748]
19. Wu C, Jin Y, Schneider T, Burnham DR, Smith PB, Chiu DT. Angew. Chem. 2010; 49:9436–9440. [PubMed: 20979060]
20. Wu C, Schneider T, Zeigler M, Yu J, Schiro PG, Burnham DR, McNeill JD, Chiu DT. J. Am. Chem. Soc. 2010; 132:15410–15417. [PubMed: 20929226]
21. Chan YH, Jin Y, Wu C, Chiu DT. Chem. Commun. 2011; 47:2820–2822.
22. Chan YH, Wu C, Ye F, Jin Y, Smith PB, Chiu DT. Anal. Chem. 2011; 83:1448–1455. [PubMed: 21244093]
23. Jin Y, Ye F, Zeigler M, Wu C, Chiu DT. ACS Nano. 2011; 5:1468–1475. [PubMed: 21280613]
24. Petkau K, Kaeser A, Fischer I, Brunsveld L, Schenning APHJ. J. Am. Chem. Soc. 2011; 133:17063–17071. [PubMed: 21913650]
25. Wu C, Hansen SJ, Hou Q, Yu J, Zeigler Ma, Jin Y, Burnham DR, McNeill JD, lson JMO, Chiu DT. Angew. Chem. Int. Ed. 2011; 50:3430–3434.
26. Ye F, Wu C, Jin Y, Chan YH, Zhang X, Chiu DT. J. Am. Chem. Soc. 2011; 133:8146–8149. [PubMed: 21548583]
27. Jin Y, Ye F, Wu C, Chan Y-H, Chiu DT. Chem. Commun. 2012; 48:3161–3163.
28. Ye F, Wu C, Jin Y, Wang M, Chan Y-H, Yu J, Sun W, Hayden S, Chiu DT. Chem. Commun. 2012; 48:1778–1780.

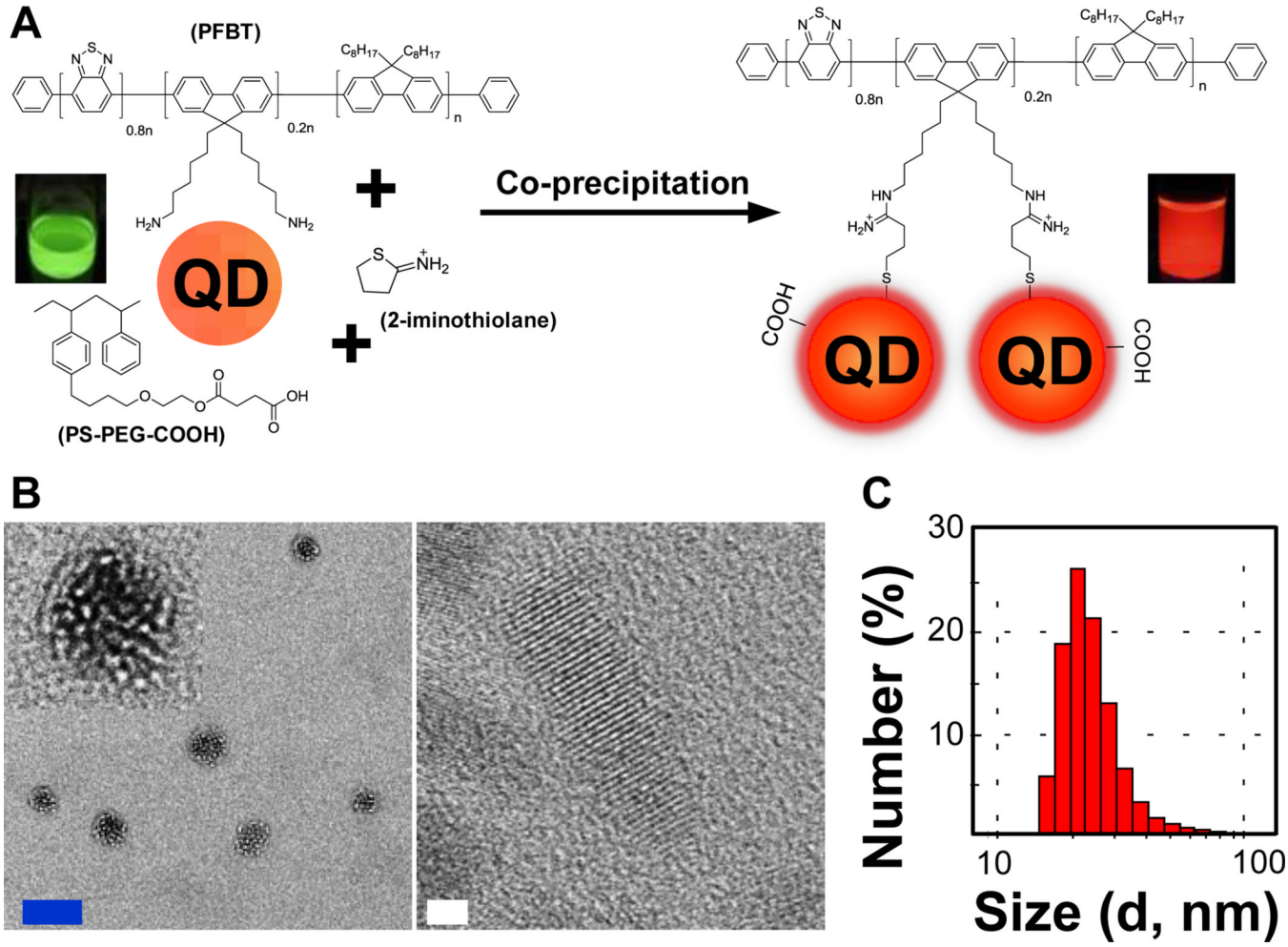

Figure 1.

(A) Schematic showing the preparation of Pdot-Qdot hydrid nanoparticles (NPs). PFBT with amino terminal groups was converted to thiols first in order to covalently bind PFBT to the surfaces of Qdots, after which the Pdot-Qdot solution was mixed with PS-PEG-COOH in THF and then co-condensed in water via nanoprecipitation under vigorous sonication to form Qdot-embedded Pdots. (B) TEM (transmission electron microscopy) images of Pdot-Qdot NPs. The inset in the upper-left corner shows the enlarged view of a single Pdot-Qdot NP. The blue and white scale bars represent 20 nm and 2 nm, respectively. (C) DLS (dynamic light scattering) measurements showing the hydrodynamic diameters (histogram; average diameter was ~25 nm) of Pdot-Qdot NPs. QD represents Qdot.

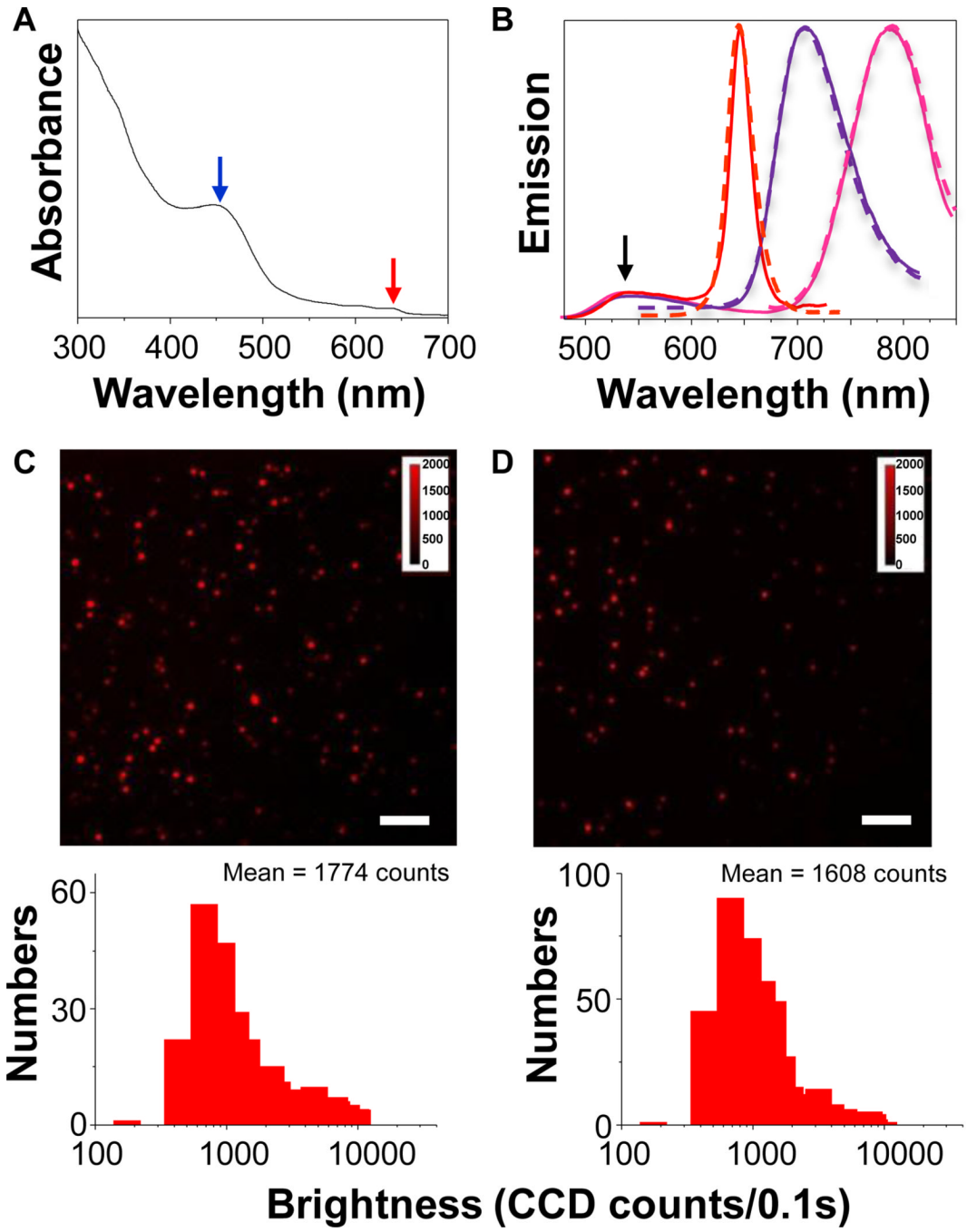

Figure 2.

Characterization of Pdot-Qdot nanoparticles (NPs). (A) UV-visible spectrum of Pdot-Qdot NPs in water. (B) Emission spectra of QD655 (dashed red line), QD705 (dashed purple line), and QD800 (dashed pink line) in decane. Emission spectra of their corresponding Pdot-Qdot forms after nanoprecipitation were shown in solid lines. (C) Single-particle fluorescence images of PFBT-DBT Pdots (PFBT blended with 4,7-di-2-thienyl-2,1,3-benzothiadiazole) (upper graph) and the corresponding histograms showing the intensity distributions (bottom graph). (D) Single-particle fluorescence images of PFBT-QD655 Pdots (upper graph) and the corresponding histograms showing the intensity distributions (bottom

graph). The scale bars are 4 μm. Each histogram is based on the measurements of at least 700 individual particles.

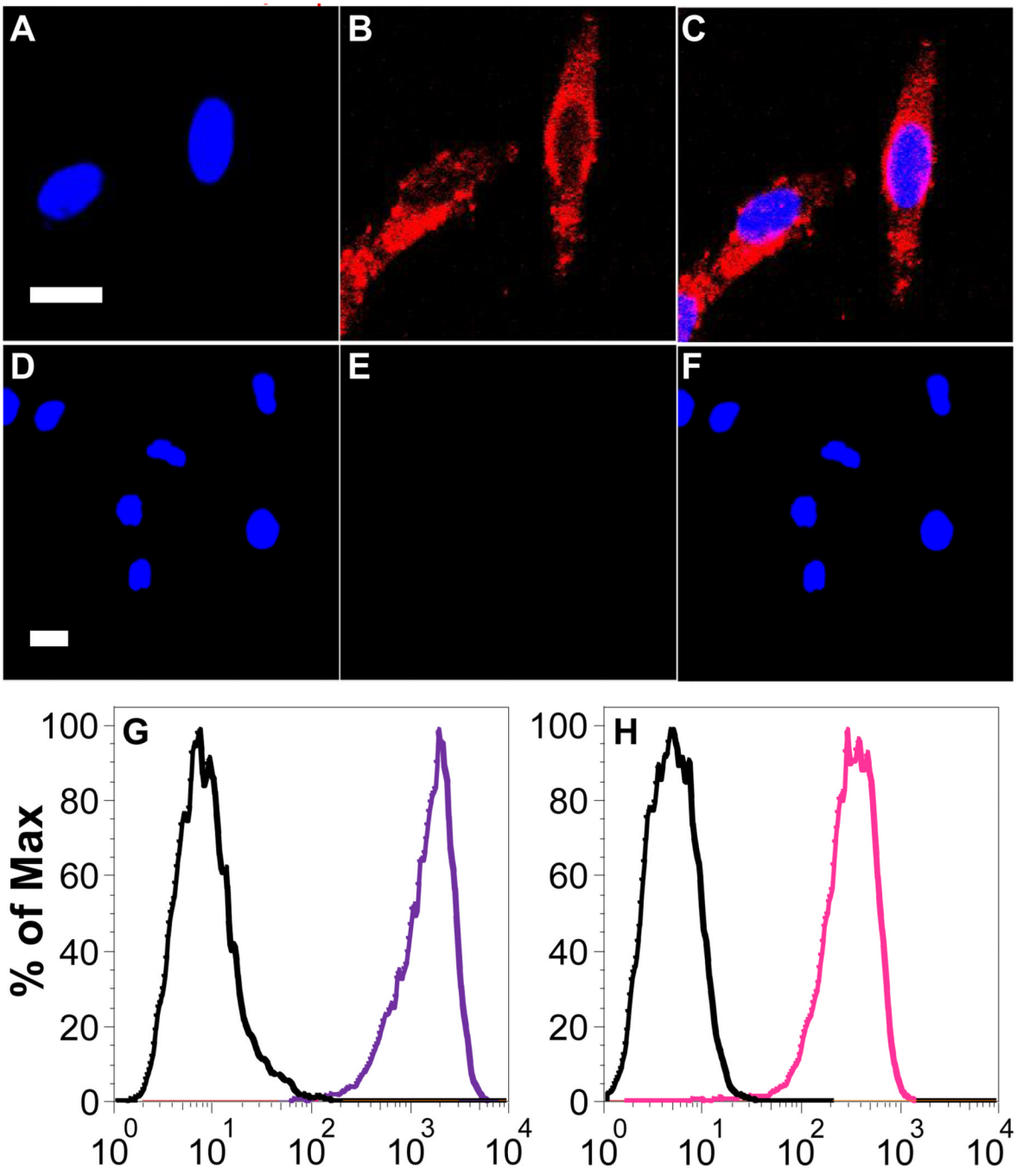

Figure 3.

Two-color confocal microscopy images of microtubules in HeLa cells labeled with Pdot-QD705-streptavidin. The blue fluorescence was from nuclear counterstain Hoechst 34580 and the red fluorescence was from Pdot-QD705-streptavidin. (A) Image of nucleus. (B) Image of microtubules. (C) The overlay of panels (A) and (B). (D–F) Images of negative control samples where cells were incubated with Pdot-QD705-streptavidin but in the absence of biotinylated primary antibody. The scale bars are 20 μm. (G–H) Flow cytometry detection of Pdot-Qdot labeled MCF-7 cells. The purple and pink lines show the fluorescence intensity distributions of Pdot-QD705-streptavidin and Pdot-QD800-

streptavidin labeled cells, respectively. The black lines represent the results of negative control samples where no primary Biotin anti-human CD326 EpCAM antibody was present.